energies

MDPI

Article

Experimental Validation of Different Control Techniques Applied to a Five-Phase Open-End Winding Induction Motor

Saad Khadar [1,*], Ameur Miloud Kaddouri [1], Abdellah Kouzou [1,2], Ahmed Hafaifa [1,2], Ralph Kennel [3] and Mohamed Abdelrahem [3,4,*]

[1] Laboratory of Applied Automation and Industrial Diagnosis, Ziane Achour University, Djelfa 17000, Algeria; amkaddouri@yahoo.fr (A.M.K.); a.kouzou@univ-djelfa.dz (A.K.); a.hafaifa@univ-djelfa.dz (A.H.)
[2] Electrical and Electronics Engineering Department, Nisantasi University, Istanbul 34398, Turkey
[3] High Power Converter Systems (HLU), Technical University of Munich (TUM), 80333 Munich, Germany; ralph.kennel@tum.de
[4] Department of Electrical Engineering, Assiut University, Assiut 71516, Egypt
* Correspondence: saad.khadar@univ-djelfa.dz (S.K.); mohamed.abdelrahem@tum.de (M.A.)

Abstract: Open-end winding five-phase induction motor (OeW-5PIM) configuration is used in industrial applications, where minimization in the total harmonic currents and high reliability are needed. The majority of the literature on OeW-5PIM topology discusses field-oriented control and direct torque control in addition to other robust control techniques such as the backstepping approach. This paper focuses on the mathematical and experimental approaches of backstepping control (BSC) and rotor-flux-oriented control (RFOC) for an OeW-5PIM topology. The space vector pulse width modulation (SVPWM) strategy is associated with the suggested control techniques to improve the dynamic performance (i.e., reducing ripple, fixed switching frequency, etc.) of the studied motor. Furthermore, the RFOC-SVPWM and BSC-SVPWM are comprehensively compared using experimental implementation under various situations such as load torque, open-phase fault, and high/low-speed operation.

Keywords: five-phase induction motor; SVPWM strategy; open-end winding; backstepping control; field-oriented control; d Space 1103 board

Citation: Khadar, S.; Kaddouri, A.M.; Kouzou, A.; Hafaifa, A.; Kennel, R.; Abdelrahem, M. Experimental Validation of Different Control Techniques Applied to a Five-Phase Open-End Winding Induction Motor. *Energies* **2023**, *16*, 5288. https://doi.org/10.3390/en16145288

Academic Editor: Federico Barrero

Received: 9 June 2023
Revised: 27 June 2023
Accepted: 6 July 2023
Published: 10 July 2023

1. Introduction

Recently, multilevel inverter configurations have been widely employed for medium/high-voltage drive systems due to their inherent advantages such as sinusoidal output currents, reduced switching losses and lower dv/dt in the output voltages, etc. [1–5]. On the other hand, multiphase machines' topology has gained interest during the last couple of decades because of their inherent benefits when compared to equivalent three-phase counterparts, such as higher robustness, lower rotor harmonic voltages, higher density of power, lower torque pulsations, better fault tolerance, higher redundancy, and greater degrees of freedom [6–13]. Therefore, it appears that multiphase machines are a strong competitor, especially in demanding high-power applications like aerospace, electric aircraft, railway traction, wind-energy conversion, ship propulsion, and other industrial applications where great reliability and redundancy are essential [9,14–16]. Due to these inherent benefits, it is feasible to combine the advantages of both structures by just using the open-end winding (OeW) structure with multilevel inverters for multiphase motor drives [2,4,5,7,17–22], where the desired configuration can be achieved by opening the neutral point of the 5PIM drive and powering both ends of the windings of the stator with a dual inverter. Due to the various benefits it possesses over a star-connected machine, the OeW design has attracted interest because of its features, such as its lower voltage stress on power switches, reduced dc-link current, multi-level waveform, higher power

factor, reduced common-mode voltage, and higher efficiency with enhanced fault-tolerant capability [2,7]. Therefore, the authors were so inspired to choose this configuration.

On the other side, researchers from all around the world have created a few control strategies for the OeW-5PIM configuration throughout the last few years of research. In [23], the authors presented a direct torque control (DTC) predicated on a new switching table to obtain a lower switching frequency. In [24], a new DTC strategy with reduced DC voltage requirements was proposed for 5PIM, where as this work proposes a method for voltage vector production that does not result in common mode voltage. But the designed strategy needs careful setup and extensive computations. In [25], a DTC technique of OeW topology fed by a matrix converter was adopted to achieve low ripple in the stator currents. Unfortunately, the DTC technique has the major disadvantage of being sensitive to stator resistance variation and load torque disturbances. In addition, one of the effective techniques for high-performance motor control is the RFOC strategy, which Blaschke proposed. This method has acquired widespread popularity in the industrial sector due to its appealing benefits of quick response and separated control of rotor flux and motor torque. In [26], the authors employed a rotor-flux-oriented control with optimized DC voltage of the OeW-5PIM topology feed by floating capacitors. In [27], an RFOC strategy with third harmonic currents was developed to generate a rectangular airgap. In [11], an indirect RFOC strategy was proposed for OeW-5PIM topology based on motor parameters estimation. However, as mentioned by the authors, the proposed technique has a large computational burden, lacks tuning criteria, and is challenging to implement.

Moreover, many non-linear techniques have been suggested in the literature such as feedback linearization control, backstepping control, and sliding mode control [2,3,7,28,29]. Between these techniques, the backstepping control predicated on the Lyapunov theory offers numerous benefits, such as high performance and fast tracking, and ensures good stability in both steady state and transient regimes [30–32]. The aim of this method is to calculate a command that ensures the stability of the overall system. Unlike most other strategies, BSC has no constraint of non-linearity, which highlights the benefits of using BSC over alternative strategies, particularly multiphase motor drives. Indeed, the BSC strategy has been success fully investigated forsix-phase IM [28] and five-phase IM [2]. Unfortunately, only simulation results were obtained in [2,28].

The experimental application of the RFOC strategy and non-linear BSC approach for the investigated motor topology supplied by a two-voltage inverter is shown in this study. In addition, this paper presents a comparative study to show the effectiveness of the suggested techniques under various situations such as load torque, open-phase fault, and high/low-speed operation. Finally, the viability and accuracy of the developed control techniques are examined in real-time implementation based on a d Space 1103 board. The study contributions can be itemized as follows:

1. Different control techniques are designed and analyzed to ensure the robustness of an OeW-5PIM drive against uncertainties and load torque that are usually present in real systems.
2. Simple control strategies are proposed to be implemented on an industrial motor control hardware system with a low computation load e in comparison with the previous works (e.g., those presented in [2,5,23,29–36]).
3. A comprehensive comparison and performance analysis is accomplished between the BSC and RFOC strategy.
4. The validation of the proposed control strategies is achieved using experimental implementation, which demonstrates the improved performance of the suggested strategies under different situations of operation.

This paper is organized as follows: Section 2 provides the 5PIM model as well as giving a review of the OeW-5PIM structure. Section 4 presents the RFOC strategy. Section 3 develops the BSC approach of the OeW-5PIM topology. Section 5 discusses the real-time results and comparison between the two control strategies. Finally, Section 6 provides a conclusion to the paper that has been presented.

2. Description of the Studied Motor Topology

This section describes the development of the 5PIM model as well as giving a review of the OeW-5PIM structure.

2.1. Modeling of the 5PIM Drive

The 5PIM model based on the field orientation law is presented in (*d-q-x-y*) frames, where the direct rotor flux is $\varphi_{rd} = \varphi_r$ and the quadratic rotor flux is supposed to be zero $\varphi_{rq} = 0$ [4], which are represented as follows [2]:

$$\begin{cases} \frac{di_{sd}}{dt} = \alpha_1.i_{sd} + \omega.i_{sq} + \alpha_2.\varphi_r + \frac{V_{sd}}{\sigma.L_s} \\ \frac{di_{sq}}{dt} = \alpha_1.i_{sq} - \omega.i_{sd} + \alpha_2.\varphi_r + \frac{V_{sq}}{\sigma.L_s} \\ \frac{di_{sx}}{dt} = -\frac{R_s}{L_{ls}} i_{sx} + \frac{V_{sx}}{L_{ls}} \\ \frac{di_{sy}}{dt} = -\frac{R_s}{L_{ls}} i_{sy} + \frac{V_{sy}}{L_{ls}} \end{cases} \quad (1)$$

$$\begin{cases} \frac{d\varphi_r}{dt} = \frac{1}{T_r}(L_{sr}.i_{sd} - \varphi_r) \\ \frac{d\omega}{dt} = -\frac{F}{J}\omega + \frac{T_{em}}{J} - \frac{T_L}{J} \end{cases} \quad (2)$$

Consequently, the developed torque formulation is as follows:

$$T_{em} = \frac{n_p.L_{sr}}{L_r} \varphi_r.i_{sq} \quad (3)$$

where i_{sd}, i_{sq}, i_{sx}, and i_{sy} denote the stator current components; V_{sd}, V_{sq}, V_{sx}, and V_{sy} are thevoltage components; T_r is the rotor time constant; L_{ls} and L_{lr} are the rotor/stator leakage inductances, respectively; L_{sr} is the magnetizing inductance; F is the viscous friction coefficient; and J is the rotor inertia. Also:

$$\alpha_1 = \frac{1}{\sigma L_s}\left(R_s + \frac{L_{sr}^2 R_r}{L_r^2}\right) ; \alpha_2 = \frac{R_r L_{sr}}{\sigma L_s L_r} ; \sigma = \frac{1 - L_{sr}^2}{L_s L_r}.$$

2.2. Electric Circuit of the OeW Configuration

The electric circuit of a 5PIM supplied by a dual-voltage source inverter (VSI) (VSI-a and VSI-b) with a separate DC is depicted in Figure 1 and will be examined in this study.

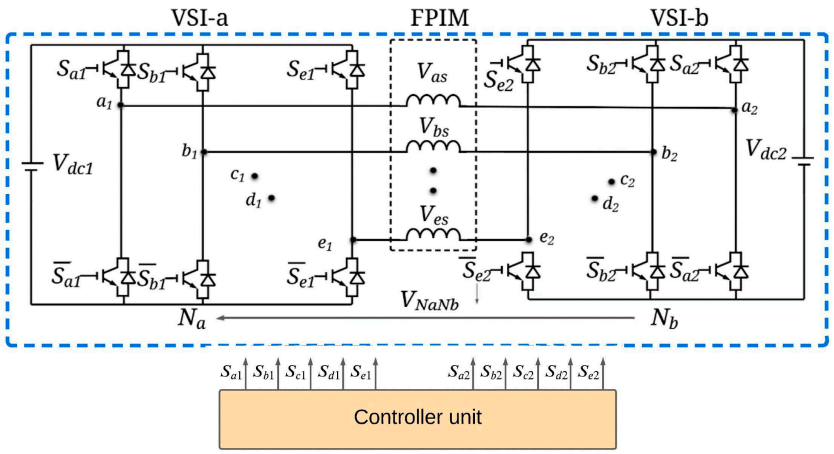

Figure 1. Electric circuit of the studied motor configuration with the separate DC sources.

On the other side, each inverter has two switches with their anti-parallel diodes. Moreover, each inverter possesses32 possible switching pulses [4]. As a consequence, as illustrated in Figure 2, there are 30 active vectors and 2null vectors. The cases for switching of the dual VSI are generated through the SVMPWM strategy, where the phase shift in the

switching situations of the inverter VSI-b is 180 degrees, while the switching states of the VSI-a are achieved in a traditional way.

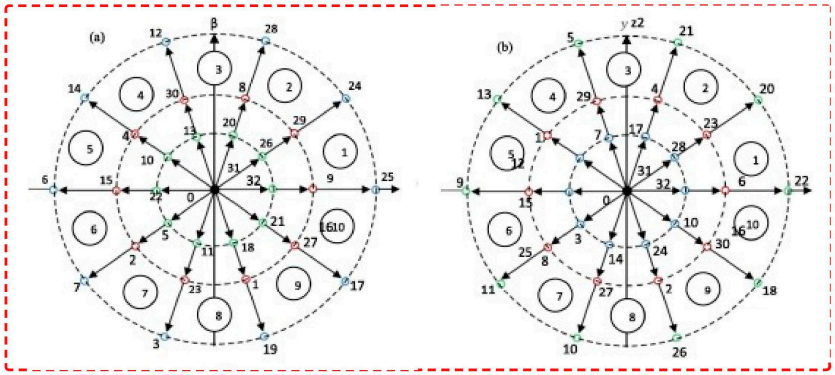

Figure 2. Space vector diagram in α-β-u-z frames.

The stator winding voltages of the 5PIM drive are represented as follows:

$$\begin{cases} V_{sa} = V_{a1Na} - V_{a2Nb} \\ V_{sb} = V_{b1Na} - V_{b2Nb} \\ V_{sc} = V_{c1Na} - V_{c2Nb} \\ V_{sd} = V_{d1Na} - V_{d2Nb} \\ V_{se} = V_{e1Na} - V_{e2Nb} \end{cases} \tag{4}$$

Additionally, the dual VSI system's DC source and switching pulses may be used to determine the output voltages of stator windings in the following ways:

$$\begin{cases} V_{VSI-a} = \begin{bmatrix} S_{a1} & S_{b1} & S_{c1} & S_{d1} & S_{e1} \end{bmatrix}^T \frac{V_{dc1}}{2} \\ V_{VSI-b} = \begin{bmatrix} S_{a2} & S_{b2} & S_{c2} & S_{d2} & S_{e2} \end{bmatrix}^T \frac{V_{dc2}}{2} \end{cases} \tag{5}$$

In fact, the only input voltages needed for a 5PIM drive are sinusoidal voltages. It is common knowledge that coupling inductances have time-varying terms; but, in order to simplify the motor model, this independence must be removed. In order to achieve this, the 5PIM model in the natural basis is subjected to Clark transformation. The matrix [T], which is the foundation for this transformation, is represented as follows:

$$[T] = \frac{2}{5}\begin{bmatrix} 1 & \cos(\theta) & \cos(2\theta) & \cos(3\theta) & \cos(4\theta) \\ 0 & \sin(\theta) & \sin(2\theta) & \sin(3\theta) & \cos(4\theta) \\ 1 & \cos(2\theta) & \cos(4\theta) & \cos(6\theta) & \cos(8\theta) \\ 0 & \sin(2\theta) & \sin(4\theta) & \sin(6\theta) & \sin(8\theta) \end{bmatrix}$$

where $\theta = 2\pi/5$.

It is obvious that based on this adequate transformation, the five-phase drive can be written in $\alpha - \beta$ and $u - z$ instead of the five components presented in the natural frame such as:

$$\begin{bmatrix} V_\alpha \\ V_\beta \\ V_u \\ V_z \end{bmatrix} = \frac{2}{5}\begin{bmatrix} 1 & \cos(\theta) & \cos(2\theta) & \cos(3\theta) & \cos(4\theta) \\ 0 & \sin(\theta) & \sin(2\theta) & \sin(3\theta) & \cos(4\theta) \\ 1 & \cos(2\theta) & \cos(4\theta) & \cos(6\theta) & \cos(8\theta) \\ 0 & \sin(2\theta) & \sin(4\theta) & \sin(6\theta) & \sin(8\theta) \end{bmatrix}\begin{bmatrix} V_{sa} \\ V_{sb} \\ V_{sc} \\ V_{sd} \\ V_{se} \end{bmatrix}$$

Thus, the voltage vectors in the stationary frames can be described as follows:

$$\begin{cases} V_{\alpha-\beta} = \frac{2}{5}\left(V_{sa} + aV_{sb} + a^2V_{sc} + a^3V_{sd} + a^4V_{se}\right) \\ V_{u-z} = \frac{2}{5}\left(V_{sa} + a^2V_{sb} + a^4V_{sc} + a^6V_{sd} + a^8V_{se}\right) \end{cases} \tag{6}$$

where $a = \exp(j2\pi/5)$.

3. Designed Control Methods

This section discusses the theoretical concept of the RFOC strategy and the BSC technique of the OeW-5PIM topology.

3.1. RFOC Method

The goal of the RFOC method is to achieve the control of the 5PIM similar to the DC machine [5,9,16], where the *d-q* stator currents may be adjusted to provide a decoupling between the motor torque and the rotor flux. Laplace transformation is used to impose the machine's equation in relation to the *d-q-x-y* frames, yielding [9]:

$$\begin{cases} V_{sd} = (R_s + s\sigma L_s)i_{sd} + sL_{sr}/L_r\varphi_r - \omega_s\sigma L_s i_{sq} \\ V_{sq} = (R_s + s\sigma L_s)i_{sq} + \omega_s L_{sr}/L_r\varphi_r + \omega_s\sigma L_s i_{sd} \\ V_{sx} = (R_s + sL_{ls})i_{sx} \\ V_{sy} = (R_s + sL_{ls})i_{sy} \end{cases} \quad (7)$$

where ω_s is the synchronous speed. The 5PIM model can therefore be represented by the block diagram that is illustrated in Figure 3.

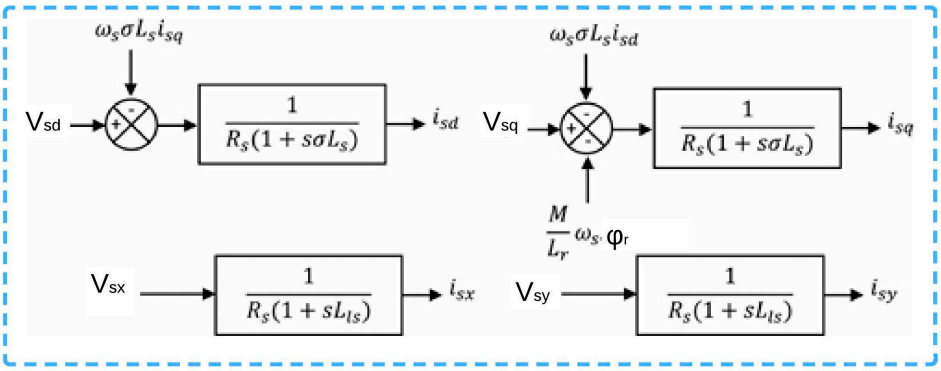

Figure 3. Decoupling system for the 5PIM drive.

The following formulas can be used to express the q-stator current and slip speed:

$$\begin{cases} i_{sq}^* = \frac{2}{5}\frac{T_{em}^*}{n_p\varphi_r}\frac{L_r}{L_{sr}} \\ \omega_{sl} = L_{sr}\frac{i_{sq}}{T_r.\varphi_r} \end{cases} \quad (8)$$

For either direct Park transformation, the angle position (θ_s) is specified as follows:

$$\begin{cases} \theta_s = \int(\omega + \omega_{sl})dt \\ \theta_s = \int\left(\omega + L_{sr}\frac{i_{sq}^*}{T_r.\varphi_r}\right)dt \end{cases} \quad (9)$$

Figure 4 displays the block diagram of the proposed RFOC approach for the OEW-5PIM structure. As can be observed, the reference currents from the errors of motor speed and rotor flux are provided by the PI controllers. These errors are supplied into the PI controllers' input block, which produces the voltage components in the *d-q-x-y* frame. The stator voltages generated by the PI controllers are transformed to the α-β frames and thereafter given to the SVM-a and SVM-b blocks, which determines the switching cases of the dual VSI. The terms e_d and e_q shown in Figure 5 are represented by:

$$\begin{cases} e_d = \omega_s\sigma L_s i_{sq} \\ e_q = -\omega_s\left(\sigma L_s i_{sd} + \frac{L_{sr}}{L_r}\varphi_r\right) \end{cases} \quad (10)$$

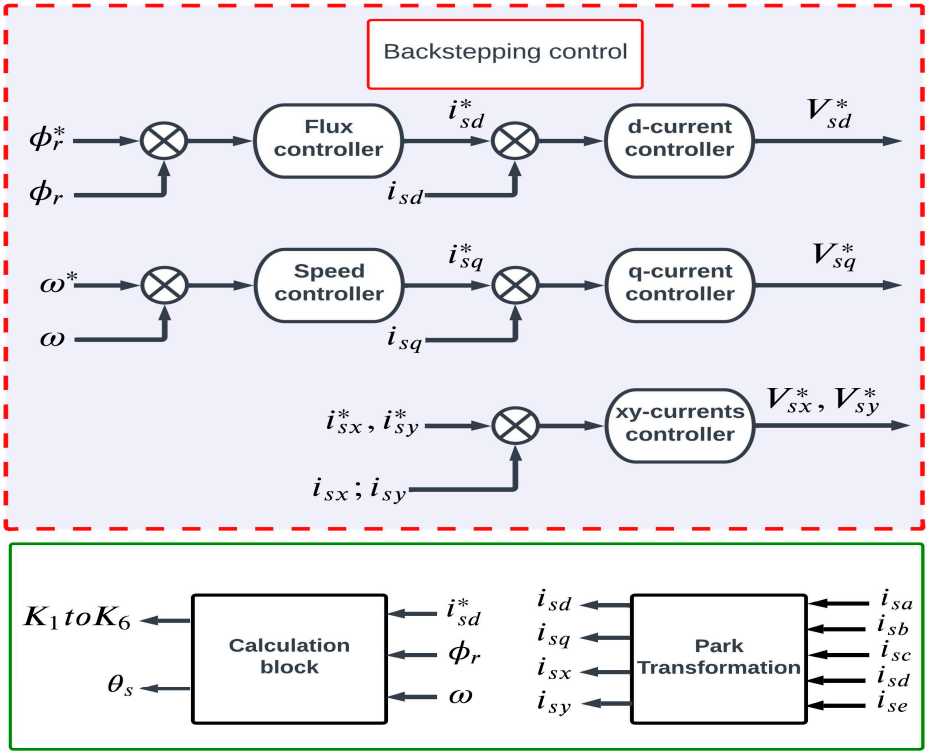

Figure 4. Basic block schematic of the BSC strategy of the OeW-5PIM topology.

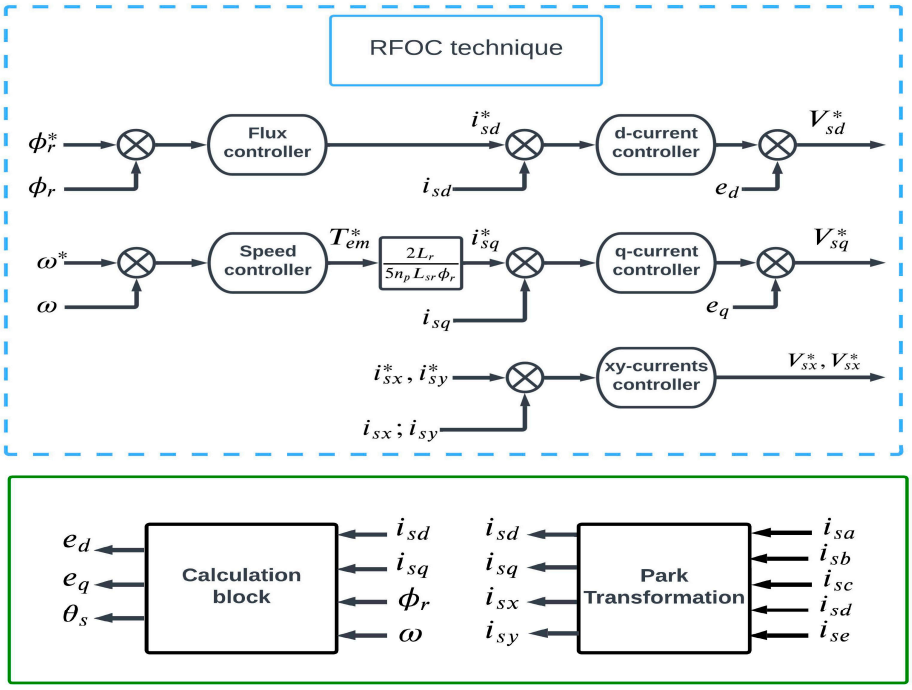

Figure 5. Basic block schematic of the RFOC strategy of the OeW-5PIM topology.

3.2. BSC Method

The fundamental goal of the BSC approach is to convert the equivalent closed-loop system into stable subsystems with order equal one [31,32], which are placed in cascade by the Lyapunov function, which guarantees the stability of each synthesis step [2]. In this paper, the proposed backstepping technique is presented in Figure 5 and it is divided into two steps:

First step: Calculation of the reference stator current: The system must adhere to the specified trajectory for each output variable in the initial phase. This is accomplished by defining the tracking errors of the rotor flux vector and the motor speed by:

$$\begin{cases} e_1 = \omega^* - \omega \\ e_2 = {\varphi_r}^* - \varphi_r \end{cases} \tag{11}$$

Then, their derivatives give:

$$\begin{cases} \dot{e}_1 = \dot{\omega}^* - \dot{\omega} \\ \dot{e}_2 = \dot{\varphi}_r{}^* - \dot{\varphi}_r \end{cases} \tag{12}$$

Accounting for (1), one can rewrite (12) as:

$$\begin{cases} \dot{e}_1 = \dot{\omega}^* - \alpha_3 \varphi_r \, i_{sq} + \frac{n_p T_L}{J} + \frac{F\omega}{J} \\ \dot{e}_2 = \dot{\varphi}_r{}^* + \frac{\varphi_r}{T_r} - \frac{L_{sr}}{T_r} i_{sd} \end{cases} \tag{13}$$

The primary goal of the necessary control is to guarantee the stability of the rotor flux and rotor speed control loops. Here is the formulation of the first Lyapunov function V_1 related to the tracking errors of rotor speed and the rotor flux vector:

$$V_1 = \frac{1}{2}\left(e_1^2 + e_2^2\right) \tag{14}$$

Using Equation (13), the derivate of V_1 is described by:

$$\dot{V}_1 = e_1\left(\dot{\omega}^* - \alpha_3 \varphi_r \, i_{sq} + \frac{n_p T_L + F\omega}{J}\right) + e_2\left(\dot{\varphi}_r^* + \frac{\varphi_r}{T_r} - \frac{L_{sr}}{T_r} i_{sd}\right) \tag{15}$$

This can be rewritten as follows:

$$\dot{V}_1 = -K_1.e_1^2 - K_2.e_2^2 \tag{16}$$

Hence, in order to provide stable tracking, K_1 and K_2 should be positive values, which gives:

$$\begin{cases} \dot{e}_1 = -K_1.e_1 \\ \dot{e}_2 = -K_2.e_2 \end{cases} \tag{17}$$

Thus, the stator currents generated by the BSC strategy can be written next as:

$$\begin{cases} i_{sd}^* = \frac{T_r}{L_{sr}}\left(K_2 e_2 + \dot{\varphi}_r^* + \frac{\varphi_r}{T_r}\right) \\ i_{sq}^* = \frac{1}{\alpha_3 \varphi_r}\left(K_1 e_1 + \dot{\omega}^* + \frac{F\omega + T_L n_p}{J}\right) \\ i_{sx}^* = 0 \\ i_{sy}^* = 0 \end{cases} \tag{18}$$

Second step: Calculation of the reference stator voltage: The reference stator voltages for the entire system are calculated in this step, and the current errors are specified as follows:

$$\begin{cases} e_3 = i_{sd}^* - i_{sd} \\ e_4 = i_{sq}^* - i_{sq} \\ e_5 = i_{sx}^* - i_{sx} \\ e_6 = i_{sy}^* - i_{sy} \end{cases} \tag{19}$$

Then, their derivatives give:

$$\begin{cases} \dot{e}_3 = \frac{di^*_{sd}}{dt} - \frac{di_{sd}}{dt} \\ \dot{e}_4 = \frac{di^*_{sq}}{dt} - \frac{di_{sq}}{dt} \\ \dot{e}_5 = \frac{di^*_{sx}}{dt} - \frac{di_{sx}}{dt} \\ \dot{e}_6 = \frac{di^*_{sy}}{dt} - \frac{di_{sy}}{dt} \end{cases} \tag{20}$$

Accounting for (1), the stator current errors can be calculated as:

$$\begin{cases} \dot{e}_3 = \frac{di^*_{sd}}{dt} - \alpha_1 i_{sd} - \omega\, i_{sq} - \alpha_2 \varphi_r - \frac{V_{sd}}{\sigma L_s} \\ \dot{e}_4 = \frac{di^*_{sq}}{dt} - \alpha_1 i_{sq} + \omega\, i_{sd} - \alpha_2 \varphi_r - \frac{V_{sq}}{\sigma L_s} \\ \dot{e}_5 = \frac{di^*_{sx}}{dt} - \frac{R_s}{L_{ls}} i_{sx} - \frac{V_{sx}}{L_{ls}} \\ \dot{e}_6 = \frac{di^*_{sy}}{dt} - \frac{R_s}{L_{ls}} i_{sy} - \frac{V_{sy}}{L_{ls}} \end{cases} \tag{21}$$

The e_1, e_2, e_3, e_4, e_5, and e_6 are taken into consideration while defining the new Lyapunov function V_2 for the stability study and are represented as follows:

$$V_2 = \frac{1}{2}\left(e_1^2 + e_2^2 + e_3^2 + e_4^2 + e_5^2 + e_6^2\right) \tag{22}$$

Hence, the derivative of the V_2 is obtained by:

$$\dot{V}_2 = \left(e_1.\dot{e}_1 + e_2.\dot{e}_2 + e_3.\dot{e}_3 + e_4.\dot{e}_4 + e_5.\dot{e}_5 + e_6.\dot{e}_6\right) \tag{23}$$

By setting (20) into (21), the V_2 can be rewritten as follows:

$$\begin{cases} V_2 = \left(-K_1 e_1^2 - K_2 e_2^2 - K_3 e_3^2 - K_4 e_4^2 - K_5 e_5^2 - K_6 e_6^2\right) \\ \quad + e_3\left(K_3 e_3 + \frac{di^*_{sd}}{dt} - \alpha_1 i_{sd} - \omega\, i_{sq} - \alpha_2 \varphi_r - \frac{V_{sd}}{\sigma L_s}\right) \\ \quad + e_4\left(K_4 e_4 + \frac{di^*_{sq}}{dt} - \alpha_1 i_{sq} + \omega i_{sd} - \alpha_2 \varphi_r - \frac{V_{sq}}{\sigma L_s}\right) \\ \quad + e_5\left(K_5 e_5 + \frac{di^*_{sx}}{dt} - \frac{R_s}{L_{ls}} i_{sx} - \frac{V_{sx}}{L_{ls}}\right) \\ \quad + e_6\left(K_6 e_6 + \frac{di^*_{sy}}{dt} - \frac{R_s}{L_{ls}} i_{sy} - \frac{V_{sy}}{L_{ls}}\right) \end{cases} \tag{24}$$

If the quantities within parentheses were selected to be equal to zero, a negative derivative of the V_2 would be obtained, whichmeans:

$$\begin{cases} K_3 e_3 + \frac{di^*_{sd}}{dt} - \alpha_1 i_{sd} - \omega\, i_{sq} - \alpha_2 \varphi_r - \frac{V_{sd}}{\sigma L_s} = 0 \\ K_4 e_4 + \frac{di^*_{sq}}{dt} - \alpha_1 i_{sq} + \omega\, i_{sd} - \alpha_2 \varphi_r - \frac{V_{sq}}{\sigma L_s} = 0 \\ K_5 e_5 + \frac{di^*_{sx}}{dt} - \frac{R_s}{L_{ls}} i_{sx} - \frac{V_{sx}}{L_{ls}} = 0 \\ K_6 e_6 + \frac{di^*_{sy}}{dt} - \frac{R_s}{L_{ls}} i_{sy} - \frac{V_{sy}}{L_{ls}} = 0 \end{cases} \tag{25}$$

Finally, the following formulae give the stator voltage references as expressions:

$$\begin{cases} lV^*_{sd} = \sigma L_s\left(K_3 e_3 + \frac{di^*_{sd}}{dt} - \alpha_1 i_{sd} - \omega\, i_{sq} - \alpha_2 \varphi_r\right) \\ V^*_{sq} = \sigma L_s\left(K_4 e_4 + \frac{di^*_{sq}}{dt} - \alpha_1 i_{sq} + \omega\, i_{sd} - \alpha_2 \varphi_r\right) \\ V^*_{sx} = L_{ls}\left(K_5 e_5 + \frac{di^*_{sx}}{dt} - \frac{R_s}{L_{ls}} i_{sx}\right) \\ V^*_{sy} = L_{ls}\left(K_6 e_6 + \frac{di^*_{sy}}{dt} - \frac{R_s}{L_{ls}} i_{sy}\right) \end{cases} \tag{26}$$

where, the positive values K_3, K_4, K_5, and K_6 are chosen to provide a quicker dynamic of motor speed, rotor flux, as well as stator currents. The block diagram of the proposed BSC for the OeW-5PIM topology is shown in Figure 6.

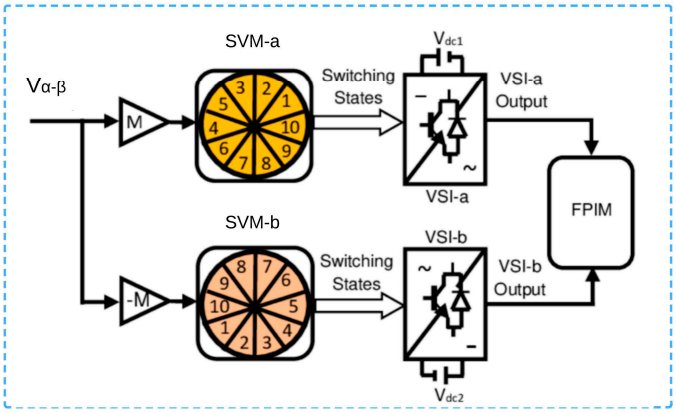

Figure 6. Principle of the dual SVPWM strategy for the OeW-5PIM topology.

3.3. SVPWM Strategy

The use of the dual VSI system requires a high number of switching states ($2^5 \times 2^5$). As a result, many SVM strategies have been developed for the OeW topology, using a modified idea of conventional modulation. In our study, we used a very simple SVPWM strategy, which was presented previously in [5]. In this block, the reference voltage is divided evenly between the two inverters, i.e., each inverter generates half of the needed voltage. Figure 6 depicts the principle of the dual SVPWM strategy (SVM-a and SVM-b). Backstepping control has recently emerged as one of the most widely used design approaches for large-scale non-linear systems.

4. Experimental Setup

The experimental setup is presented in Figure 7, and it essentially consists of a d Space 1103 control board, a hysteresis dynamometer, a5PIM of 2.2 kW, a host computer, four three-phase inverters, adaptation interfaces (15 V), a speed sensor, current sensors, and an oscilloscope Yokogawa DL850.

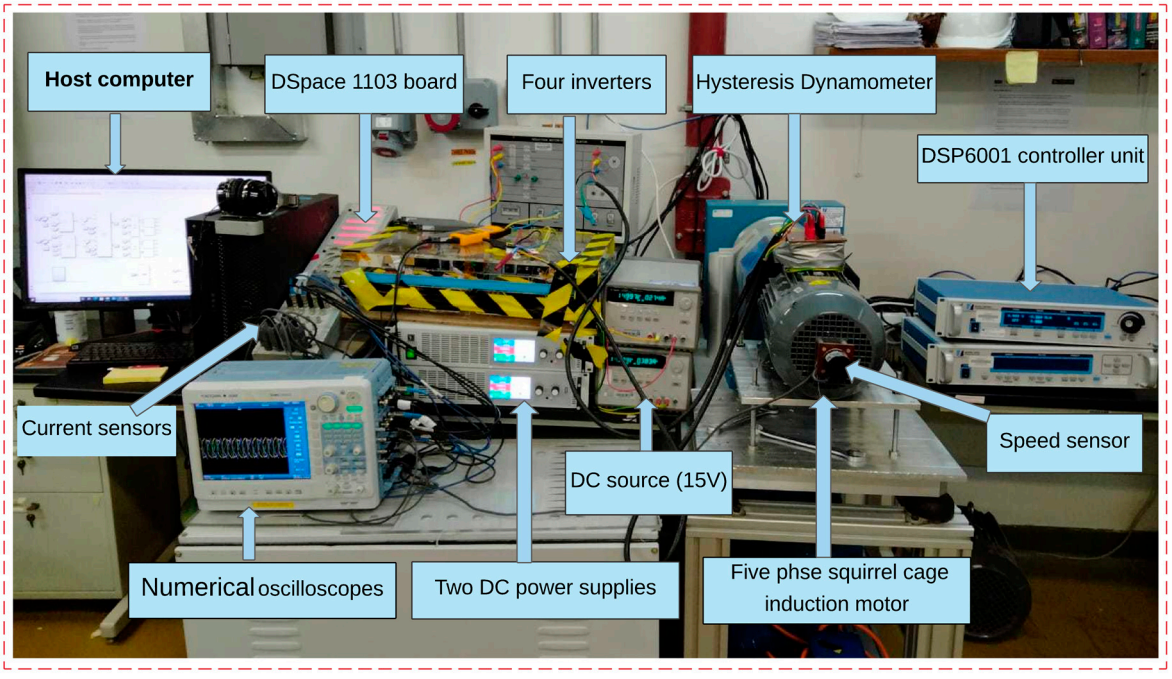

Figure 7. Block diagram of the experimental setup.

A Hysteresis Dynamometer HD-815-8NA was mounted on the rotor shaft of the motor to vary the load torque disturbances using a DSP6001 controller. The five-phase stator currents are sensed by a Yokogawa current probe which are connected in series with the inverter terminals and sent to the DSP through its analog boards. The phase voltages produced by the dual VSI system are calculated from the DC-bus voltage and switching states, which results in are duction in the required number of sensors and the cost of the control system. The signal of the real rotor speed is also measured through the 60-bit encoder for comparison purposes with the reference speed. The experimental results of the sensorless control algorithms were obtained by using a numerical oscilloscope (Yokogawa DL850) which was linked to the real-time interface.

In the present application, for validation of the proposed control, it was built under Mat lab/Simulink. Furthermore, this control algorithm was implemented on the DSP-1103 board control to generate the switching states of the dual inverter using Control Desk Manager Software. It is well known that such software presents a perfect graphical interface between Simulink blocks and d SPACE that allows for ensuring the generation of the control signals to control and visualize in real time different signals reflecting the concerned variables as outputs which are related to the Simulink environment (the sensors' output signals).

It is important to clarify that the chosen sampling time applied to the implemented system has an important influence on the quality of the resulting signals and their accuracy. Indeed, in this study, major attention was directed to the phase currents and the developed electromagnetic torque, independently of the type of implemented control algorithms. Indeed, due to the limitations imposed by real-time implementation constraints and the complexity of the used control algorithms, a high value of the sampling time of 80 µ swasapplied without affecting the dynamic quality of the control and the feedback signals' execution, while the transistor switching frequency was kept within 20 kHz. It is important to mention that the simulation results are presented for each control algorithm to prove their effectiveness, whereas the experimental results for the same algorithm are presented for the validation of the obtained results through a simulation and to check their practical effectiveness.

5. Simulation and Experimental Results

For verification of the benefits of the control algorithms given in this study for ensuring the control of the OeW-5PIM topology, the simulation and experimental results are provided to assess the performance of the suggested control algorithms under various situations such as variable load torque, open-phase faults, and high/low-speed operation. The reference flux value was fixed in all tests to 1 Wb. The 5PIM parameters are given in Table 1.

Table 1. The parameters of the 5PIM drive.

Parameter	Value
Rated power	2.2 kW
Number of poles	1
Rotor resistance	2.7 Ω
Stator resistance	2.9 Ω
Magnetizing inductance	785.2 mH
Rotor inductance	796.4 mH
Stator inductance	796.4 mH
Moment of inertia	0.007 Kg·m^2
Friction coefficient	0.0018 N·m·s

5.1. First Test

To show the feasibility of the proposed control algorithms, the first conducted test was carried out under load torque variation. The reference speed was set to 157 rad/s. Figures 8 and 9 display the numerous simulation results of the control algorithms for BSC

and RFOC beside each other. Figure 8 presents the OeW-5PIM performance of the RFOC strategy with the load torque application at t = 2 s: (a) speed responses; (b) speed error; (c) developed torque; and (d) stator currents, while Figure 9 shows the OeW-5PIM performance of the BSC strategy under the same conditions (a) speed responses; (b) speed error; (c) developed torque; and (d) stator currents.

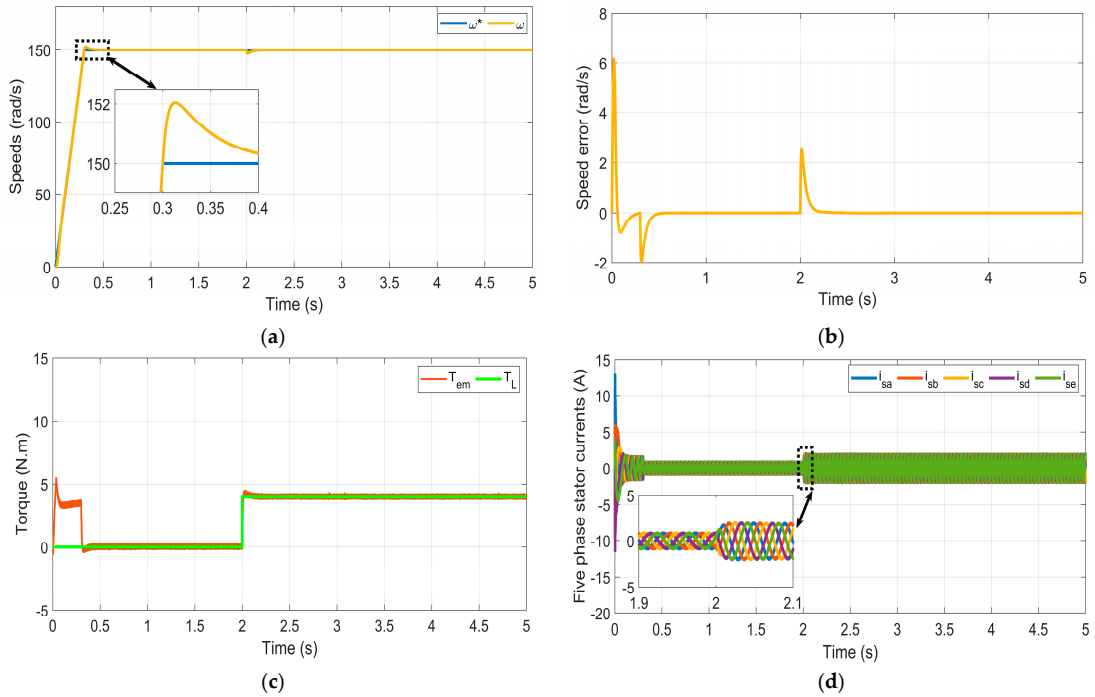

Figure 8. Simulation results of the RFOC strategy for the OeW-5PIM topology under load torque variation.

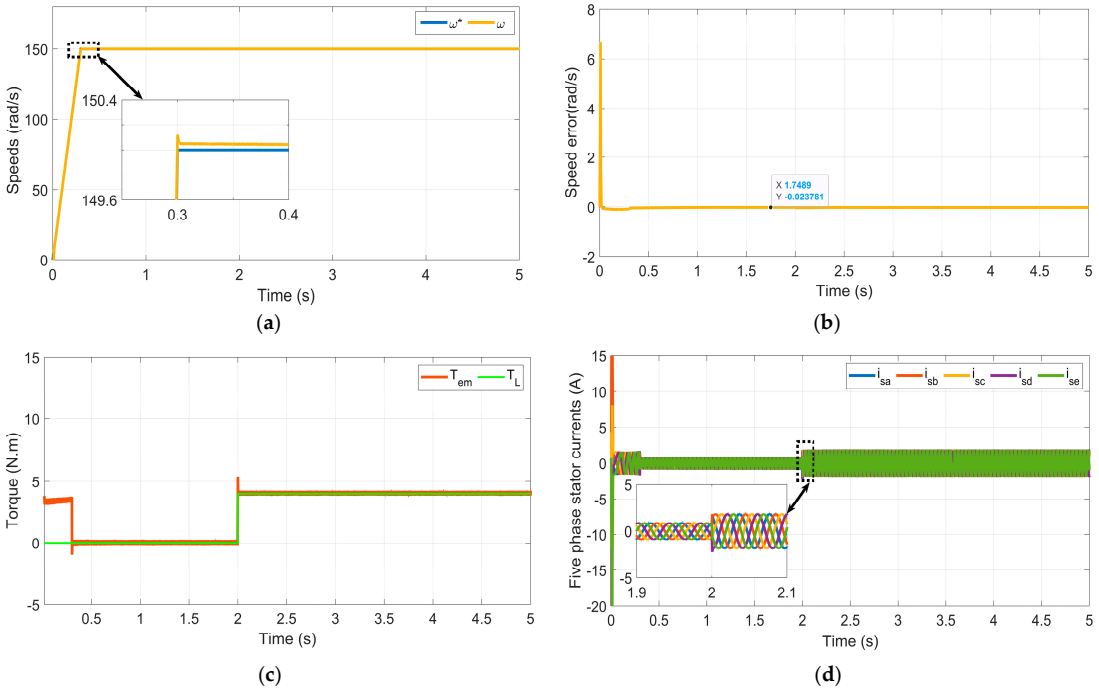

Figure 9. Simulation results of the BSC strategy for the OeW-5PIM topology under load torque variation.

The obtained experimental results are exhibited in Figures 10 and 11,where Figure 10 represents the OeW-5PIM performance of the RFOC strategy: (a) speed responses, speed error, and developed torque and (b) stator currents, while Figure 11 shows the OeW-5PIM performance of the BSC strategy: (a) speed responses, speed error, and developed torque and (b) stator currents. These results show the validation of the effectiveness of the obtained simulation results for the designed control algorithms under load torque variation.

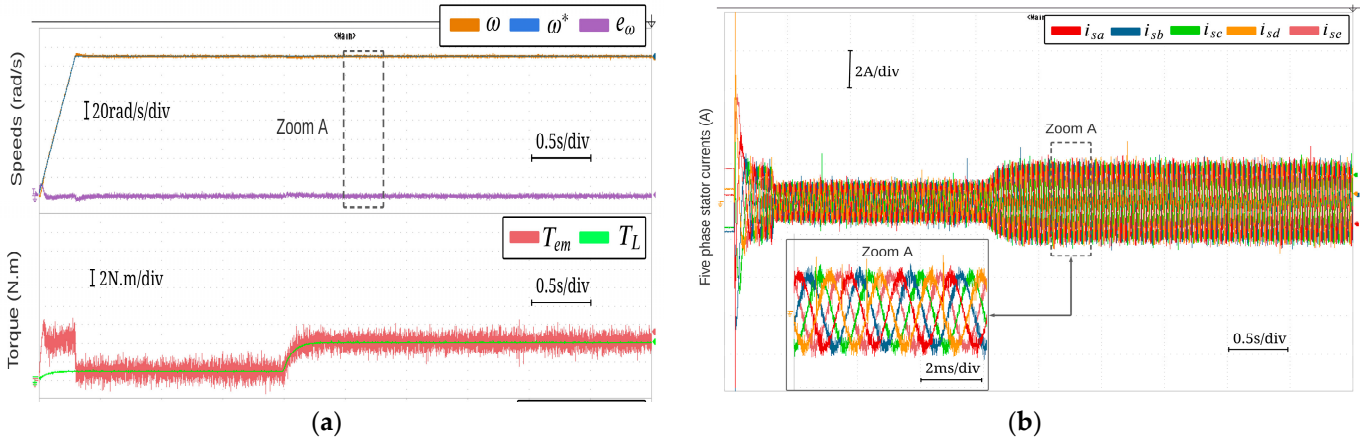

Figure 10. Experimental results of the RFOC strategy for the OeW-5PIM topology under load torque variation.

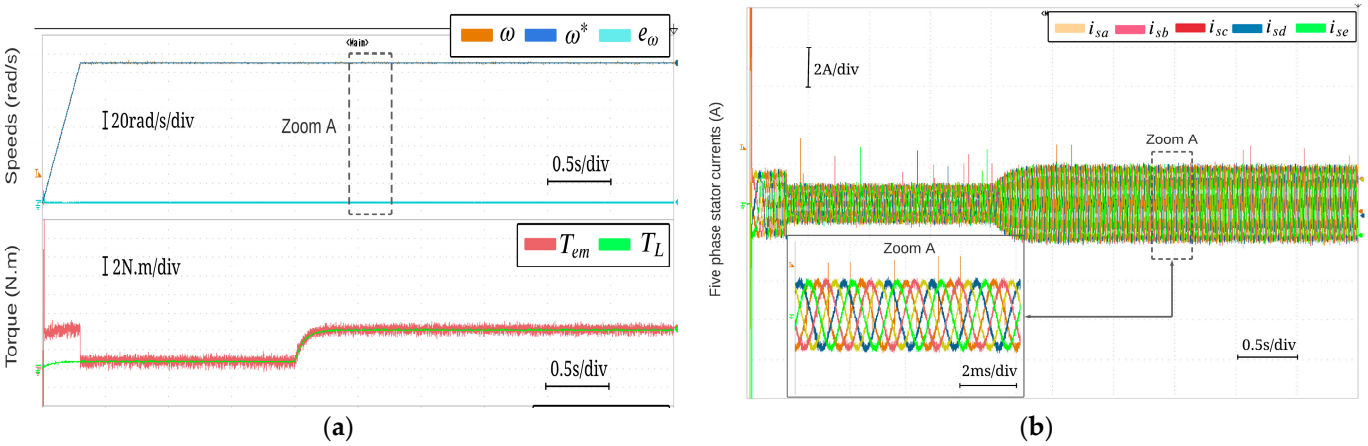

Figure 11. Experimental results of the BSC strategy for the OeW-5PIM topology under load torque variation.

5.2. Second Test

To evaluate the effectiveness of the proposed control algorithms of the OeW-5PIM under open-phase faults, a special test was carried out with constant load torque (4 N·m at t = 2 s). Figures 12 and 13 show the simulation results of the control techniques for BSC and RFOC. Figure 12 presents the OeW-5PIM performance of the RFOC strategy with an open-phase fault at t = 3 s: (a) speed responses; (b) speed error; (c) developed torque; and (d) stator currents, while Figure 13 represents the OeW-5PIM performance of the BSC strategy:(a) speed responses; (b) speed error; (c) developed torque; and (d) stator currents.

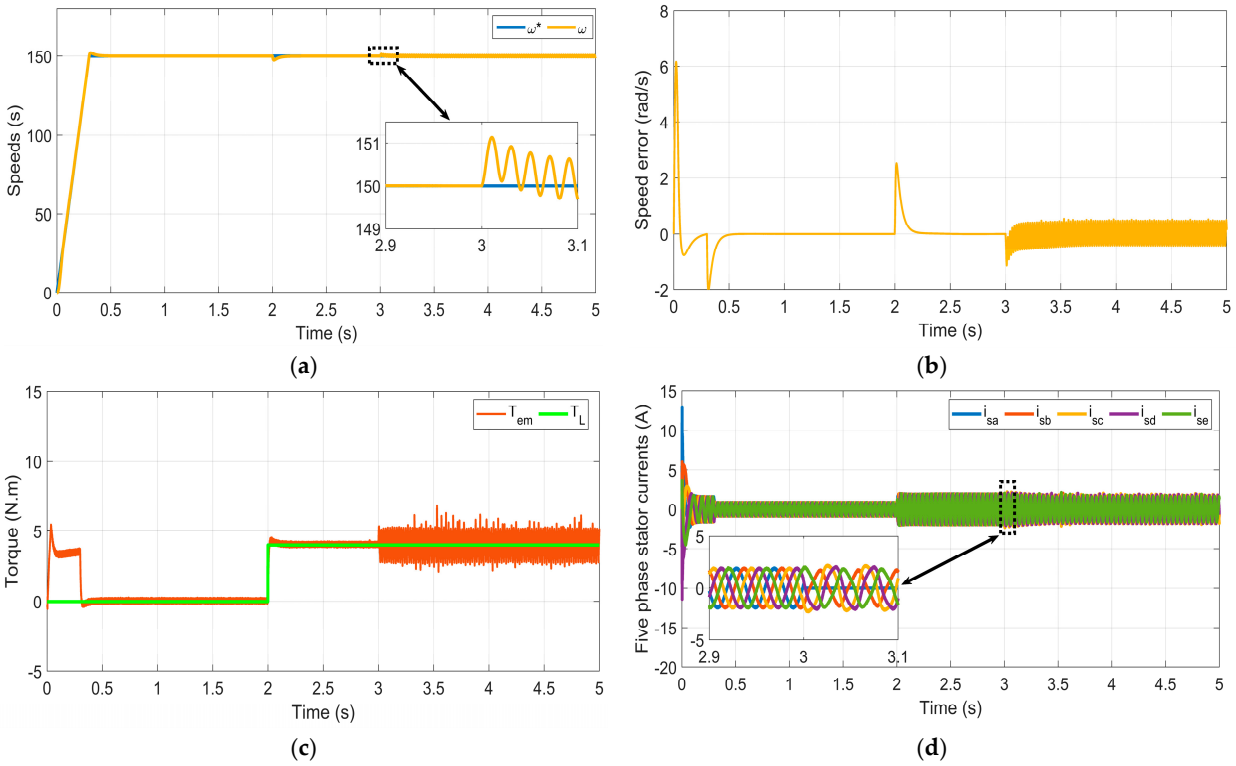

Figure 12. Simulation results of the RFOC strategy for the OeW-5PIM topology with an open-phase fault.

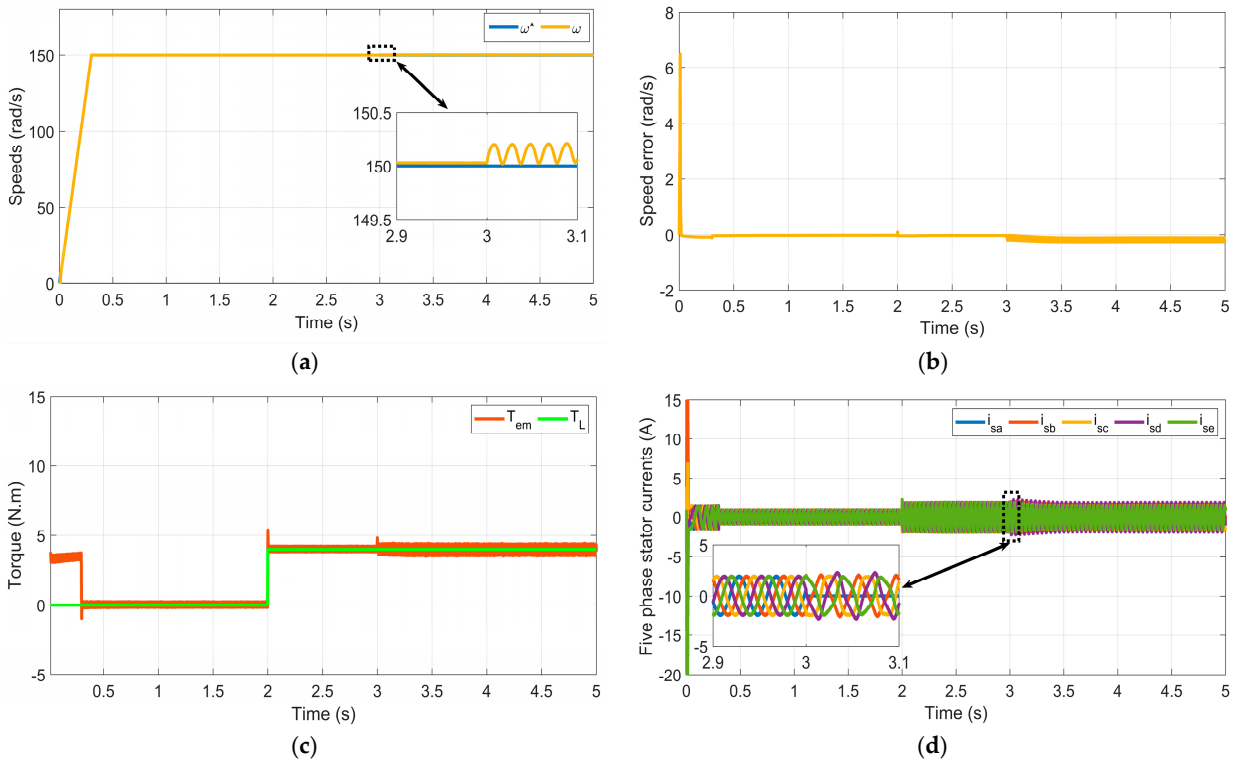

Figure 13. Simulation results of the BSC strategy for the OeW-5PIM topology with an open-phase fault.

The obtained experimental results of the OeW-5PIM's performance under an open-phase fault are shown in Figures 14 and 15: (a) speed response and the developed torque

response; and (b) is the five phase stator currents. These results demonstrate the reliability of the simulation results for the developed control algorithms when there is an open-phase fault.

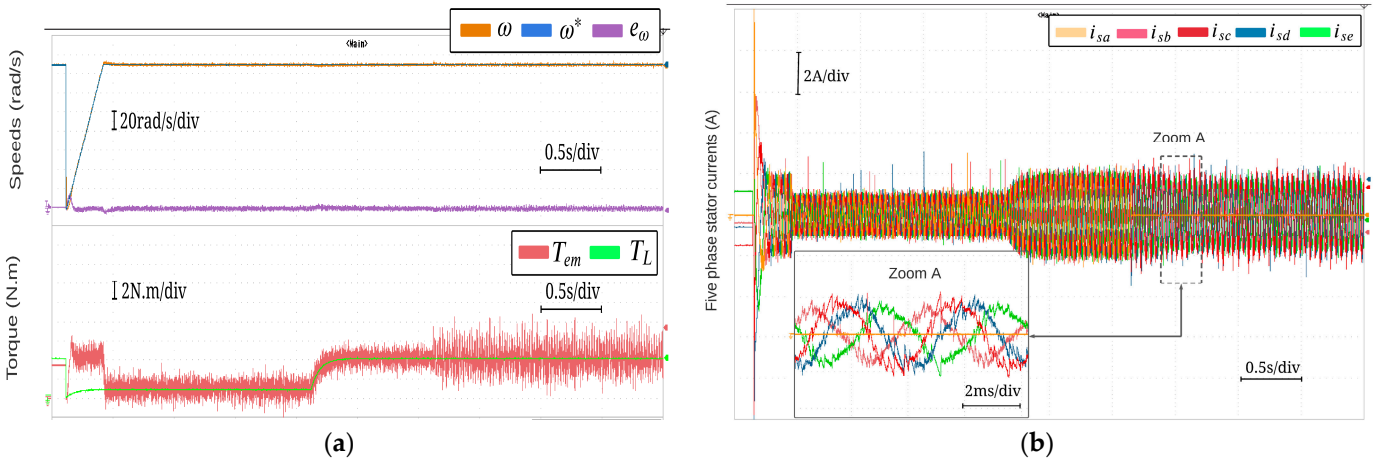

(**a**) (**b**)

Figure 14. Experimental results of the BSC strategy for the OeW-5PIM topology with an open-phase fault.

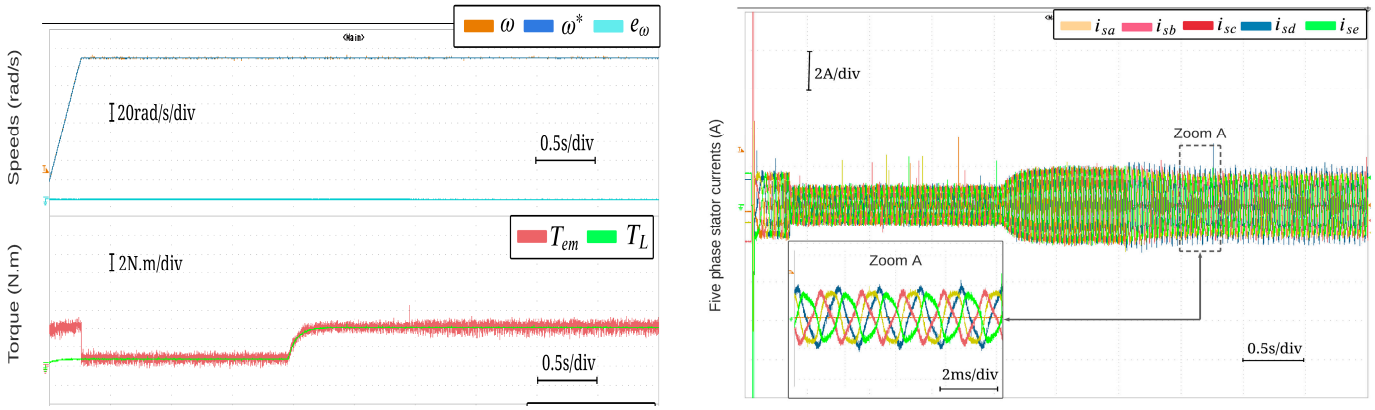

(**a**) (**b**)

Figure 15. Experimental results of the BSC strategy for the OeW-5PIM topology with an open-phase fault.

5.3. Third Test

We sought to evaluate the effectiveness of the suggested control strategies under different speed values. Here, there are three steps for the reference speed change, from 0 to 150 rad/s and 150 rad/s to −150 rad/s. Figures 16 and 17 show the simulation results of the OeW-5PIM's performance for BSC and RFOC during reversal speed. The results present the responses of (a) the speed responses; (b) the speed error; (c) the developed torque; and (d) the stator currents.

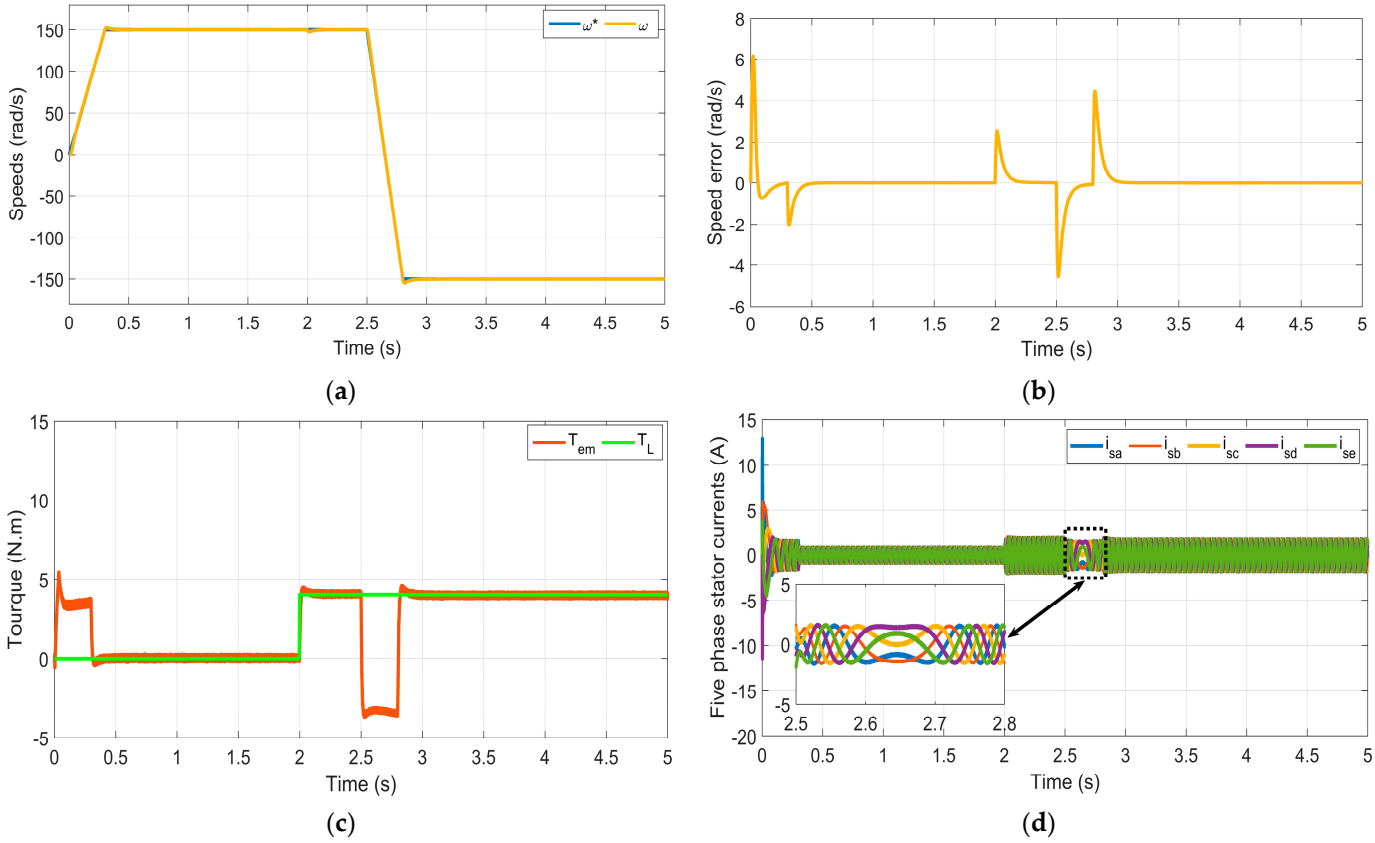

Figure 16. Simulation results of the RFOC strategy for the OeW-5PIM topology under reversal speed.

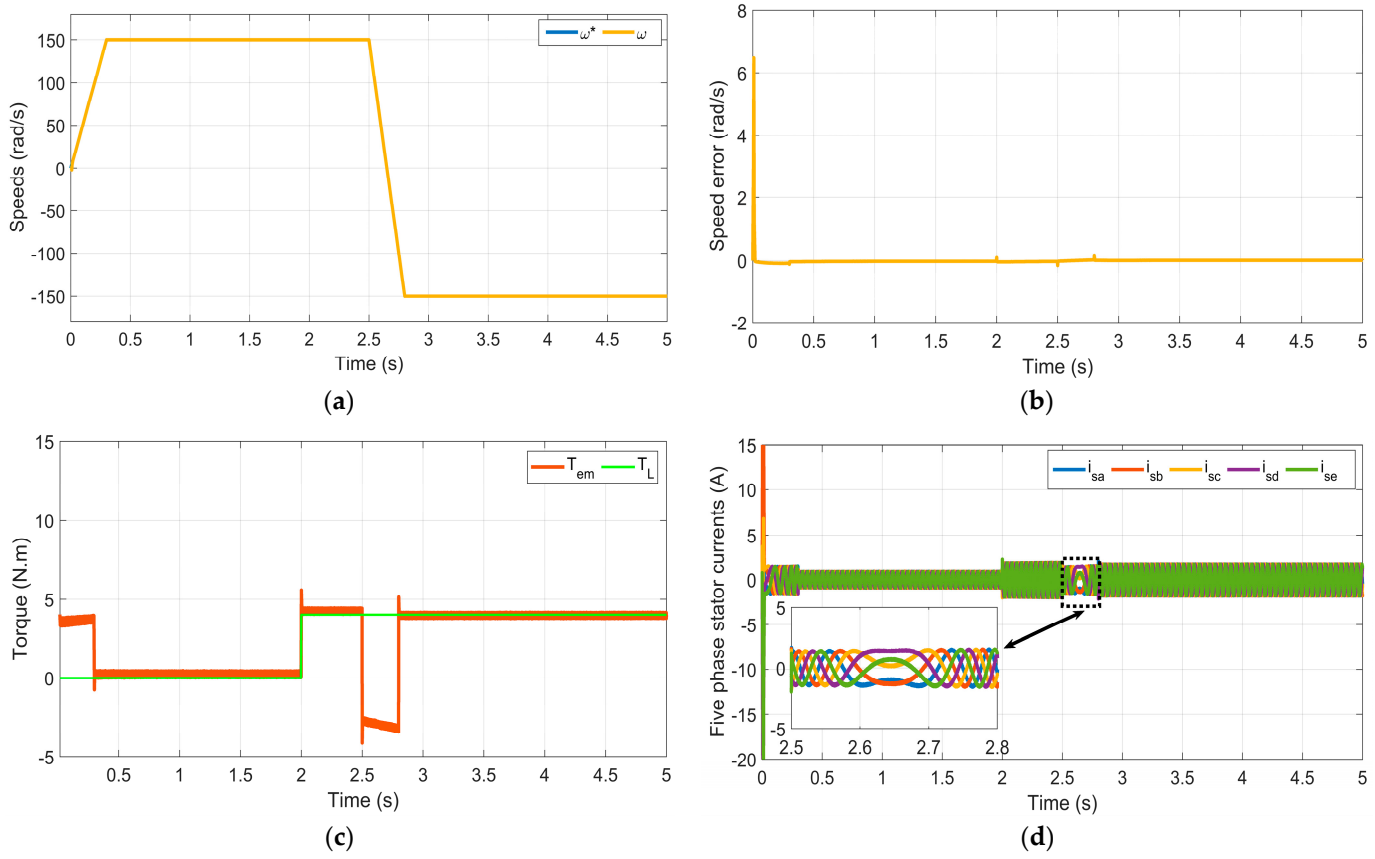

Figure 17. Simulation results of the BSC strategy for the OeW-5PIM topology under reversal speed.

The experimental results of the OeW-5PIM's performance during reversal speed are presented in Figures 18 and 19: (a) speed response and the developed torque response; and (b) is the five phase stator currents. These results present the validity of the simulation results for the developed control algorithms even under rotor speed variation.

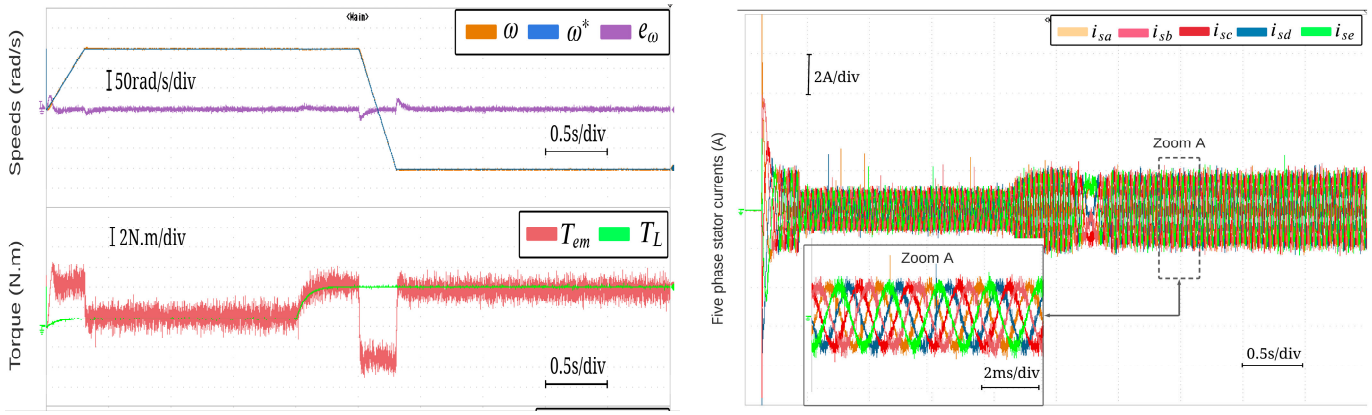

(**a**) (**b**)

Figure 18. Experimental results of the BSC strategy for the OeW-5PIM topology under reversal speed.

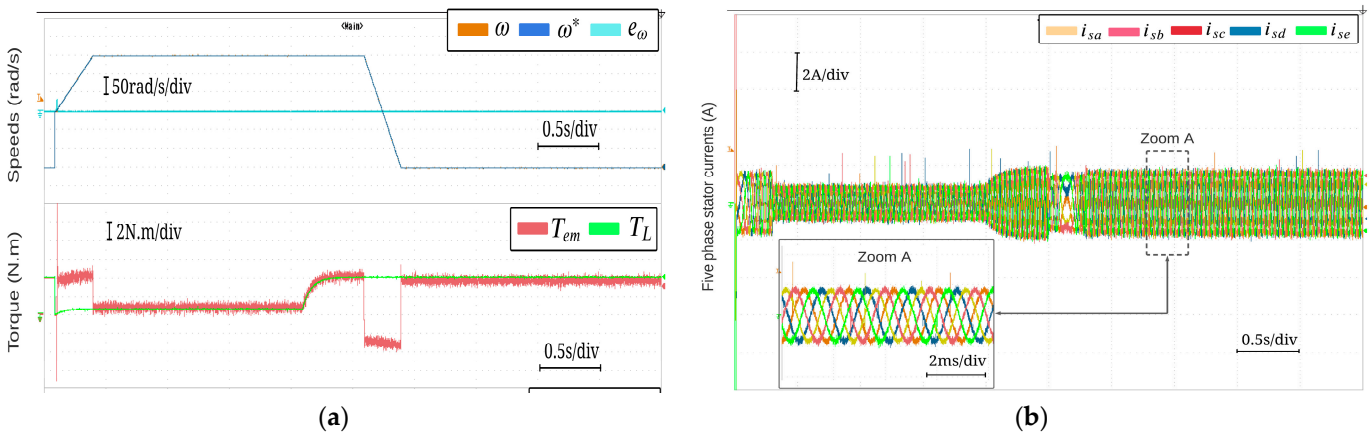

(**a**) (**b**)

Figure 19. Experimental results of the BSC strategy for the OeW-5PIM topology under reversal speed.

6. Discussion

This part provides a quick comparison of the control approaches discussed in this work. Table 2 shows the brief comparison of several factors discovered by using the experimental and simulation results of the designed control techniques. The comparison is based on many factors, including dynamic behavior, open-phase fault, stability characteristics, design options for the controller, and the implementation complexity.

Dynamic behavior: The motor speed tracks the reference speed with excellent performance while changes in the reference speed and load do not affect the speed tracking. Therefore, the speed error is less when compared to the obtained results in [4,8–12,29]. It can be said that the obtained results clearly prove the accuracy of the backstepping controller against sudden changes in the specified reference speed and load torque compared to the RFOC technique. At the same time, the torque developed by the motor behaves in a similar way to the controlled systems within an acceptable range of ripples compared to the obtained results in previous research works such as in [5–8,11,24,26], where it can be observed clearly that the torque amplitude changes according to the speed step changes and load torque variation. Furthermore, the d-q rotor flux demonstrates excellent decoupling between the motor torque and the rotor flux even under reversal speed. On the other side, the amplitudes of the five-phase stator currents increased after the load torque

changed. In addition, as shown in the zoomed-in window, these currents have balanced sinusoidal signals.

Open-phase fault: It can be seen that the open-phase fault introduced some small fluctuations in the rotor speed and some fluctuations occur in the form of oscillations in the electromagnetic torque, which are basically directly due to the residual asymmetry at the level of the motor stator circuit.

Stability characteristics: Pole compensation is used for the RFOC technique and Lyapunov stability is used for the BSC strategy in the stability study. Both techniques exhibit steady performance, with BSC showing quicker convergence compared to other techniques such as those presented previously in [2,30–32].

Implementation complexity: Because the PI controller, in contrast to the BSC strategy, only has two controller parameters, the RFOC was simpler to implement and design. As a result, the complexity of the BSC's implementation is substantially higher.

Table 2. Comparison of the designed control techniques.

	RFOC Strategy	BSC Strategy
Rising time (rad/s)	2	0.12
Dynamic performance (Response time (s))	0.15	0.04
Open-phase fault (Ripple (N·m))	2.8	1.2
Possibilities of controller design	Low	High
Stability proprieties	Good	High
Complexity of implementation	Low	High

7. Conclusions

In this paper, different control techniques based on the SVPWM strategy were suggested for the control of the studied motor topology. The superiority and efficacy of the suggested control approaches were investigated through real-time implementation by using the d Space 1103 board. Based on the obtained results in this paper, it can be noted clearly that the proposed non-linear backstepping control using the SVPWM strategy can ensure suitable and competitive control for multiphase motors, especially under the topology presented in this paper. At the same time, it can be said that the proposed control allows for the avoidance of computational complexity burdens, and furthermore, it can be easily implemented using low-cost microcontrollers. Based on these aforementioned advantages, it can be concluded that the proposed solution can be a promising candidate in industrial applications, where high reliability and avoidance of operation interruption are ensured such as in electric vehicles, aerospace vehicles, complex industrial processes, and electric ship propulsion. In addition, the non-linear BSC strategy was compared to the RFOC technique in a wide range of operation modes, where by this comparison demonstrated that the BSC strategy provides excellent performance compared to an RFOC approach in terms of quicker response and rise time. Indeed, high performance and good tracking are provided by the backstepping strategy compared with the other RFOC strategies of OeW-5PIM topology in both dynamic and steady state situations. However, the complexity of implementation for BSC still has drawbacks, making it challenging to adjust the gains of the control scheme. Our future research work will further study the optimized torque control via the backstepping approach using a genetic algorithm for the studied motor topology.

Author Contributions: Conceptualization, S.K., A.M.K. and A.K.; methodology, S.K., M.A. and A.H.; software, S.K., A.M.K. and A.H.; validation, S.K. and A.K.; formal analysis, S.K., A.M.K. and A.K.; investigation, S.K.; resources, S.K.; data curation, S.K.; writing—original draft preparation, S.K.; writing—review and editing, S.K., R.K. and M.A. visualization, S.K.; supervision, R.K. and M.A.; project administration, R.K. and M.A. All authors have read and agreed to the published version of the manuscript.

Funding: This research received no external funding.

Data Availability Statement: Not applicable.

Conflicts of Interest: The authors declare no conflict of interest.

References

1. Liu, G.; Geng, C.; Chen, Q. Sensorless Control for Five-Phase IPMSM Drives by Injecting HF Square-Wave Voltage Signal into Third Harmonic Space. *IEEE Access* **2020**, *8*, 69712–69721. [CrossRef]
2. Khadar, S.; Kouzou, A.; Hafaifa, A.; Iqbal, A. Investigation on SVM-Backstepping sensorless control of five-phase open-end winding induction motor based on model reference adaptive system and parameter estimation. *Eng. Sci. Technol. Int. J.* **2019**, *22*, 1013–1026.
3. Mohamed, I.D.; Ahmed, A.E.; Ahmed, M.M.; Radu, B.; Shehab, A. Zero-/low-speed operation of multiphase drive systems with modular multilevel converters. *IEEE Access* **2019**, *7*, 14353–14365.
4. Khadar, S.; Abdelaziz, A.Y.; Elbarbary, Z.M.S.; Mossa, M.A. An Improved Sensorless Nonlinear Control Based on SC-MRAS Estimator of Open-End Winding Five-Phase Induction Motor Fed by Dual NPC Inverter: Hardware-in-the-Loop Implementation. *Machines* **2023**, *11*, 469. [CrossRef]
5. Payami, S.; Behera, R.K.; Iqbal, A. DTC of three-level NPC in verter fed five-phase induction motor drive with novel neutral point voltage balancing scheme. *IEEE Trans. Power Electron.* **2018**, *33*, 1487–1500. [CrossRef]
6. Hosseyni, A.; Trabelsi, R.; Mimouni, M.F.; Iqbal, A.; Alammari, R. Sensorless sliding mode observer for a five-phase perma-nent magnet synchronous motor drive. *ISA Trans.* **2015**, *58*, 462–473. [CrossRef]
7. Holakooie, M.H.; Ojaghi, M.; Taheri, A. Direct Torque Control of Six-phase Induction Motor with a Novel MRAS-Based Stator Resistance Estimator. *IEEE Trans. Ind. Electron.* **2018**, *65*, 7685–7696. [CrossRef]
8. Khadar, S.; Abu-Rub, H.; Kouzou, A. Sensorless Field-Oriented Control for Open-End Winding Five-Phase Induction Motor with Parameters Estimation. *IEEE Open J. Ind. Electron. Soc.* **2021**, *2*, 266–279. [CrossRef]
9. Echeikh, H.; Trabels, R.; Iqbal, A.; Mimouni, M.F. Adaptive direct torque control using Luenberger-sliding mode observer for online stator resistance estimation for five-phase induction motor drives. *Electr. Eng.* **2018**, *100*, 1639–1649. [CrossRef]
10. Khadar, S.; Kouzou, A.; Rezaoui, M.M.; Hafaifa, A. Fault-tolerant sensorless sliding mode control by parameters estimation of an open-end winding five-phase induction motor. *Model. Meas. Control* **2019**, *92*, 6–15. [CrossRef]
11. Taheri, S.; Hai-Peng, R.; Chun-Huan, S. Sensorless Direct Torque Control of the Six-Phase Induction Motor by Fast Reduced Order Extended Kalman Filter. *Complexity* **2020**, *2020*, 8985417. [CrossRef]
12. Echeikh, H.; Trabels, R.; Iqbal, A.; Mimouni, M.F. Real time implementation of indirect rotor flux-oriented control of a five-phase induction motor with novel rotor resistance adaption using sliding mode observer. *J. Frankl. Inst.* **2018**, *355*, 2112–2141. [CrossRef]
13. Mossa, A.M.; Quynh, N.; Echeikh, H.; Do, T.D. Deadbeat-Based Model Predictive Voltage Control for a Sensorless Five-Phase Induction Motor Drive. *Math. Probl. Eng.* **2020**, *2020*, 30. [CrossRef]
14. Bojoi, R.; Cavagnino, A.; Tenconi, A.; Vaschetto, S. Control of shaft-line-embedded multiphase starter/generator for aero-engine. *IEEE Trans. Ind. Electron.* **2016**, *63*, 641–652. [CrossRef]
15. De-Lillo, L.; Empringham, L.; Wheeler, P.; Khwan, S.; Gerada, C.; Othman, M.; Huang, X. Multiphase power converter drive for fault-tolerant machine development in aerospace applications. *IEEE Trans. Ind. Electron.* **2010**, *57*, 575–583. [CrossRef]
16. Bojoi, R.; Cavagnino, A.; Cossale, M.; Tenconi, A. Multiphase starter generator for a 48 V mini-hybrid power train: Design and testing. *IEEE Trans. Ind. Appl.* **2016**, *52*, 1750–1758.
17. Maia, A.C.N.; Jacobina, C.B.; Freitas, N.B.D.; Pinheiro, I.F.M. Open-end multilevel six-phase machine drive system with five three leg converters. *IEEE Trans. Ind. Appl.* **2017**, *53*, 2271–2281. [CrossRef]
18. Haifeng, W.; Xinzhen, W.; Xiaoqin, Z.; Xibo, Y. Model Predictive Current Control of Nine-Phase Open-End Winding PMSMs with an Online Virtual Vector Synthesis Strategy. *IEEE Trans. Ind. Electron.* **2023**, *70*, 2199–2208.
19. Wang, H.; Wu, X.; Zheng, X.; Yuan, X. Virtual Voltage Vector Based Model Predictive Control for a Nine-Phase Open-End Winding PMSM with a Common DC Bus. *IEEE Trans. Ind. Electron.* **2022**, *69*, 5386–5397. [CrossRef]
20. Du, Y.; Ji, J.; Zhao, W.; Tao, T.; Xu, D. Self-Adapted Model Predictive Current Control for Five-Phase Open-End Winding PMSM with Reduced Switching Loss. *IEEE Trans. Power Electron.* **2022**, *37*, 11007–11018. [CrossRef]
21. Surana, P.; Majumder, M.G.; Resalayyan, R.; Gopakumar, K.; Umanand, L.; Jarzyna, W. A Fault-Tolerant 24-Sided Voltage Space Vector Structure for Open-End Winding Induction Motor Drive. *IEEE Trans. Power Electron.* **2022**, *37*, 10738–10746. [CrossRef]
22. Dong, Z.; Wen, H.; Song, Z.; Liu, C. 3-D SVM for Three-Phase Open-End Winding Drives with Common DC Bus. *IEEE Trans. Power Electron.* **2023**, *38*, 9340–9346. [CrossRef]
23. Ramahlingam, S.; Bin Jidin, A.; Victor Raj, L.R.; Bin Said, M.A.; Bin Abdul, K. Improved Performance of DTC for 5-Phase Induction Machine Using Open-End Topology. In Proceedings of the 2014 IEEE International Conference on Energy Conversion (CENCON), Johor Bahru, Malaysia, 13–14 October 2014.
24. Mavila, P.C.; Rajeevan, P.P. A new direct torque control scheme for five phase open-end winding induction motor drives with reduced DC voltage requirement. In Proceedings of the 2020 IEEE International Conference on Power Electronics, Smart Grid and Renewable Energy (PESGRE2020), Cochin, India, 2–4 January 2020; IEEE: Piscataway, NJ, USA, 2020; pp. 1–6.
25. Muthu, R.; Govindarajan, K.; Anbazhagan, D.; Mahadevan, S. Direct Torque Control of Open–End Winding Induction Motor using Matrix Converter. In Proceedings of the 2014 IEEE International Conference on Power Electronics (IICPE), Kurukshetra, India, 8–10 December 2014.

26. Sun, X.; Liu, Z.; Jiang, D.; Kong, W. Control of Five-Phase Open-End Induction Machine Drive Topology with Floating Capacitors at Optimized DC Voltage. In Proceedings of the 2019 IEEE International Conference on Energy Conversion Congress and Exposition (ECCE), Baltimore, MD, USA, 29 September–3 October 2019.
27. Listwan, J.; Pieńkowski, K. Field-oriented control of five-phase induction motor with open-end stator winding. *Arch. Electr. Eng.* **2016**, *65*, 395–410. [CrossRef]
28. Fatemi, J.R.; Abjadi, N.R.; Soltani, J.; Abazari, S. Speed sensorless control of a six-phase induction motor drive using backstepping control. *IET Power Electron.* **2014**, *7*, 114–123. [CrossRef]
29. Ammar, A.; Kheldoun, K.; Metidji, B.; Ameid, T.; Azzoug, Y. Feedback linearization based sensorless direct torque control using stator flux MRAS-sliding mode observer for induction motor drive. *ISA Trans.* **2020**, *98*, 382–392. [CrossRef]
30. Hamida, M.A.; de Leon, J.; Glumineau, A. Experimental sensorless control for IPMSM by using integral backstepping strategy and adaptive high gain observer. *Control Eng. Pract.* **2017**, *59*, 64–76. [CrossRef]
31. Yang, Q.; Peng, D.; Cai, J.; Guo, D.; He, Z. Adaptive backstepping control for permanent magnet linear motors against uncertainties and disturbances. *Proc. Inst. Mech. Eng.* **2023**. [CrossRef]
32. Khadar, S.; Kouzou, A.; Benguesmia, H. Remedial Robust Control of Five-Phase Fault-Tolerant Induction Motor with Open-End Winding using Reduced-Order Transformation Matrices. *Model. Meas. Control A* **2019**, *92*, 16–23. [CrossRef]
33. Gonzalez-Prieto, I.; Duran, M.; Aciego, J.; Martin, C.; Barrero, F. Model predictive control of six-phase induction motor drives using virtual voltage vectors. *IEEE Trans. Ind. Electron.* **2018**, *65*, 27–37. [CrossRef]
34. Khan, M.R.; Atif, I. Experimental investigation of five-phase induction motor drive using extended Kalman-filter. *Asian Power Electron. J.* **2009**, *3*, 1–7.
35. Strankowski, P.; Guzinski, J.; Morawiec, M.; Lewicki, A.; Wilczynski, F. Sensorless five-phase induction motor drive with third harmonic injection and inverter output filter. *Bull. Pol. Acad. Sci. Tech. Sci.* **2020**, *68*, 133369.
36. Tavana, N.R.; Dinavahi, V. Real-time nonlinear magnetic equivalent circuit model of induction machine on FPGA for hardware-in-the-loop simulation. *IEEE Trans. Energy Convers.* **2016**, *31*, 520–530. [CrossRef]